Vol 16 No 1, January 2007
1009-1963/2007/16(01)/0258-08

Chinese Physics

© 2007 Chin. Phys. Soc.
and IOP Publishing Ltd

# Electric and magnetic behaviour in double doped $La_{2/3+4x/3}Sr_{1/3-4x/3}Mn_{1-x}Mg_xO_3$*

Qu Zhe(屈 哲), Pi Li(皮 雳)†, Fan Ji-Yu(樊济宇), Tan Shun(谭 舜), Zhang Bei (张 贝), Zhang Meng(张 锰), and Zhang Yu-Heng (张裕恒)

*Structure Research Laboratory, University of Science and Technology of China, Hefei* 230026, *China*

(Received 28 March 2006; revised manuscript received 13 June 2006)

The double-doped $La_{2/3+4x/3}Sr_{1/3-4x/3}Mn_{1-x}Mg_xO_3$ samples with fixed $Mn^{3+}/Mn^{4+}$ ratio equal to 2/1 are investigated by means of magnetism and transport measurements. Phase separation is observed at temperature higher than $T_c^{onset}$ for $x = 0.10$ and 0.15. For $x = 0.10$, rather strong phase separation induces drastic magnetic random potential and results in the localization of carriers. Thus, the variable-range hopping process dominates. For other samples, there is no or only weak phase separation above $T_c^{onset}$. Thus, thermal activation mechanism is responsible for the high temperature transport behaviour. For $x = 0.20$ and 0.25, unexpected AFM behaviour is observed at low temperature. All these results are well understood by considering the special role of the "double-doping".

**Keywords:** perovskite manganites, double doping, phase separation, variable-range hopping mechanism

**PACC:** 7540C, 7630, 5225F, 7530V

## 1. Introduction

Perovskite manganites with the $ABO_3$ structure have been intensively studied recently due to their fascinating properties and potential application. Various doping methods are adopted to study the delicate interplay in these strongly correlated electron systems. It is well known that there is paramagnetic–ferromagnetic (PM–FM) transition accompanied by insulator–metal (IM) transition in the A-site doping cases.[1−12] This type of doping results in the change of the bond length and bond angle of the system. In addition, the random potential can also be induced. Thus, the cluster-spin glass state can be formed in the B-layers. These effects all lead to the decrease of $T_c$. However, there is also PM–FM transition without IM transition when Mn ions is substituted.[13−15] The doping of the nonmagnetic ions (such as Zn, Mg, Cu etc.) blocks the long-range magnetic interaction directly. The doping of magnetic ions (such as Fe, Co, Ni, Cr etc.) can even introduce the complex superexchange (SE) or double-exchange (DE) effect. These phenomenon are intensively explored.[16−21]

It is well known that the $Mn^{3+}/Mn^{4+}$ ratio plays an important role in the properties of the manganites with colossal magnetoresistance effect. Generally, divalent cation substitution for Mn in manganites, such as $Mg^{2+}$ doping in $La_{2/3}Sr_{1/3}MnO_3$, will increase the content of $Mn^{4+}$, which will change the $Mn^{3+}/Mn^{4+}$ ratio. Such a "single-doping" will result in the change of the $Mn^{3+}/Mn^{4+}$ ratio and then bring about additional effects. Therefore, in order to study the doping effect individually, we design a series of "double-doped" samples with $Mn^{3+}/Mn^{4+}$ ratio fixed at 2/1 with respect to different doping level.

In this paper, double doped $La_{2/3+4x/3}Sr_{1/3-4x/3}Mn_{1-x}Mg_xO_3$ ($0.05 \leq x \leq 0.25$) are studied by the means of magnetism and transport measurements and compared with the single doped $La_{2/3}Sr_{1/3}Mn_{1-x}Mg_xO_3$ ($0.05 \leq x \leq 0.20$).[22] The non-magnetic ion $Mg^{2+}$ is chosen to substitute Mn because the radius of $Mg^{2+}$ (72 pm) is close to that of $Mn^{3+}$(64.5 pm) among those divalent ions. Therefore the crystal lattice would not be distorted greatly by the $Mg^{2+}$ doping and the heavily doped samples could be obtained. For the single doped samples, the $Mn^{3+}/Mn^{4+}$ ratio changes from 2:1 ($x = 0.00$) to 1:2 ($x = 0.20$). And for the double doped samples, this ratio will not change and keeps at the constant value of 2:1 for various $x$. For the double doped sample with $x = 0.25$, the Sr

*Project supported by the National Natural Science Foundation of China (Grant Nos 10504029 and 10334090), and the State Key Project of Fundamental Research, China (Grant No 001CB610604).

†Corresponding author. E-mail: pili@ustc.edu.cn

is substituted by La completely. Therefore, it is the maximum doping level for the double doped series. The results observed in the double doped samples are found to be much different from that in the single doped cases.

## 2. Experimental details

Polycrystalline samples $La_{2/3+4x/3}Sr_{1/3-4x/3}Mn_{1-x}Mg_xO_3$ ($0.05 \leq x \leq 0.25$) were prepared by conventional solid-state reaction method. The starting materials, $La_2O_3$ (preheated at 800 °C firstly), $SrCO_3$, $MnO_2$ and MgO, were mixed and heated in air at 900 °C for 12 h, 1200 °C for 24 h and 1300 °C for 12 h with intermediate grinding. Finally, the powder was pressed into pellets and sintered in air at 1380 °C for 30 h. All samples were cooled down to room temperature in the furnace. The quality of the samples was examined by means of secondary electron image (SEI) and composition image (COMPO) using a JOEL-6700F Scanning Electron Microscope(SEM). The temperature $T$ dependence of magnetization ($M$) under both zero field cooling (ZFC) and 0.01 Tesla field cooling (FC) was measured by a Lakeshore 9300 vibrating sample magnetometer (VSM). The magnetic field (H) dependence of magnetization was also measured by VSM. The temperature ($T$) dependence of resistivity was measured by standard four-contact method from 5 K to 320 K. The electron spin resonance (ESR) spectra are collected on a Bruker-200D spectrometer.

## 3. Results and discussion

### 3.1. Structure

In Fig.1, the XRD patterns of $La_{2/3+4x/3}Sr_{1/3-4x/3}Mn_{1-x}Mg_xO_3$ ($0.05 \leq x \leq 0.25$) reveal that the samples are all in the pure phase with standard $ABO_3$ perovskite structure, identical to that of $La_{2/3}Sr_{1/3}Mn_{1-x}Mg_xO_3$ ($0.05 \leq x \leq 0.20$).[22]

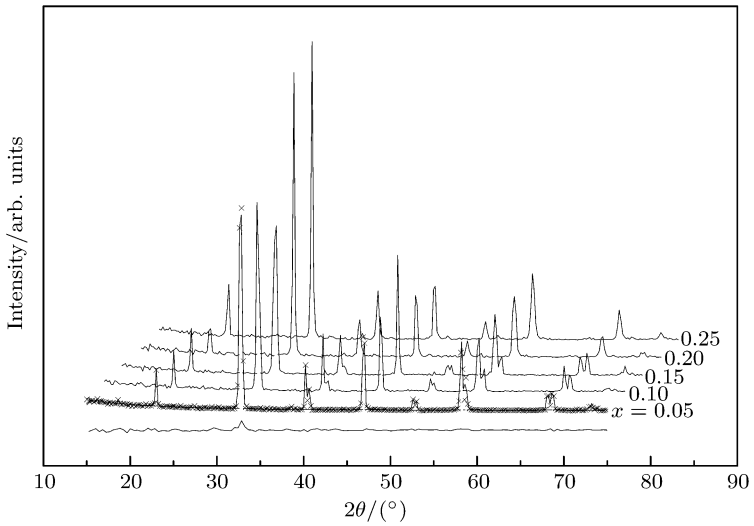



**Fig.1.** X-ray-diffraction patterns of $La_{2/3+4x/3}Sr_{1/3-4x/3}Mn_{1-x}Mg_xO_3$ ($0.05 \leq x \leq 0.25$)). Symbols '×' represent fit of a Rietveld analysis.

The structure is in the rhombohedral phase for lower Mg doping and there is a transition from rhombohedral to orthorhombic phase with increasing doping level ($x \geq 0.20$). With increasing $x$, the $Sr^{2+}$ ($r = 126$ pm) content decreases but the $La^{3+}$ ($r = 117$ pm) content increases. Therefore, the tolerance factor[23,24]

$$t = \frac{R_A + R_O}{\sqrt{2}(R_B + R_O)} \quad (1)$$

decreases with increasing $x$ (from 0.934 for $x = 0.05$ to 0.914 for $x = 0.25$, as summarized in Table 1 By means of the Rietveld method, we calculated the lattice parameters, Mn–O bond length $L_{Mn-O}$ and Mn–O–Mn bond angle $\theta_{Mn-O-O}$ for double doped samples, also shown in Table 1. From Table 1, one can find that the parameters for $x \leq 0.15$ change in a way opposite to that for $x > 0.15$. This is because the samples with $x \leq 0.15$ is in rhombohedral phase, while the samples with $x > 0.15$ is in orthorhombic phase. The XRD patterns prove that no impurity phase is detected up to $x = 0.25$. To confirm the quality of the samples, we

perform the SEM studies on the double doped sample $LaMn_{0.75}Mg_{0.25}O_3$ of highest doping level, the images are shown in Fig.2. The SEI image at magnification of 2000× is shown in Fig.2(a), the COMPO images at magnifications of 2000 and 15000× are shown in Figs.2(b) and 2(c), respectively. From the SEI image we can find that the sample crystallized very well and there is no educt. From the COMPO image, one can find that the brightness is almost uniform, which is sensitive to the composition in the scanned region. This indicates that the sample is homogeneous and Mg ions substitute Mn ions uniformly. These results are easy to understand because Mg cannot form $MgO_6$ octahedron like the $MnO_6$ octahedron. The Mg ion is forced to enter the Mn-site of the perovskite and the strain is induced. If two or more Mg ions should occupy close-by Mn-sites, the local strain energy would increase drastically. Therefore, the Mg ions have to disperse and occupy the Mn-sites uniformly to lower the local strain.

**Table 1.** Cell parameters, Mn–O bond length ($L_{\mathrm{Mn-O}}$), Mn–O–Mn bond angle ($\theta_{\mathrm{Mn-O-Mn}}$), $t$ factor and $T_{\mathrm{cd}}^{\mathrm{onset}}$ of the double doped samples; $T_{\mathrm{cs}}^{\mathrm{onset}}$ of the single doped samples are also given. The data of the single doped samples are quoted from Ref.[22].

| $x$ | 0.05 | 0.10 | 0.15 | 0.20 | 0.25 |
|---|---|---|---|---|---|
| $a$/Å | 5.5161 | 5.5251 | 5.5258 | 5.4962 | 5.5012 |
| $b$/Å | 5.5161 | 5.5251 | 5.5258 | 7.7914 | 7.8004 |
| $c$/Å | 13.3626 | 13.3580 | 13.3440 | 5.5350 | 5.5293 |
| $L_{\mathrm{Mn-O}}$/Å | 1.9577 | 1.9631 | 1.9639 | 1.9598 | 1.9570 |
| $\theta_{\mathrm{Mn-O-Mn}}$/(°) | 166.0 | 164.4 | 163.9 | 167.3 | 170.4 |
| $t$ | 0.9337 | 0.9289 | 0.9240 | 0.9190 | 0.9142 |
| $T_{\mathrm{cs}}^{\mathrm{onset}}$/K | 340 | 340 | 320 | 320 | |
| $T_{\mathrm{cd}}^{\mathrm{onset}}$/K | 310 | 200 | 130 | 110 | 100 |

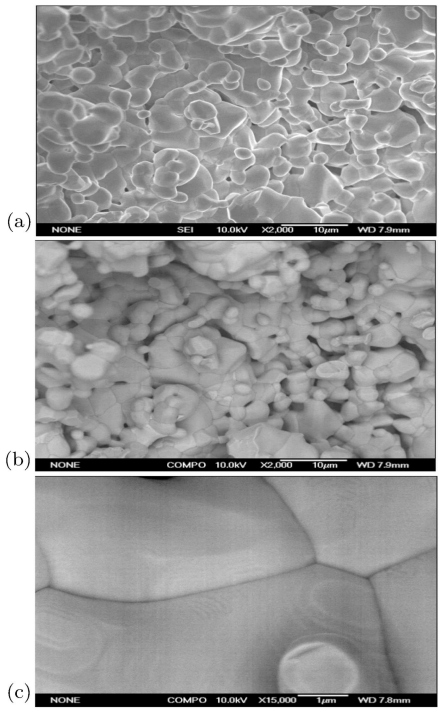



**Fig.2.** SEM images of $LaMn_{0.75}Mg_{0.25}O_3$: (a) the SEI image at magnification of 2000×; (b), (c) the COMPO images at magnifications of 2000 and 15000×, respectively.

## 3.2. Macromagnetism

The $M$–$T$ relations after ZFC and FC of the double doped samples $La_{2/3+4x/3}Sr_{1/3-4x/3}Mn_{1-x}Mg_xO_3$ ($0.05 \leq x \leq 0.25$) are shown in Fig.3. As shown in Fig.3 and summarized in Table 1, the $T_{\mathrm{cd}}^{\mathrm{onset}}$, which is defined as the onset temperature of PM–FM phase transition of the double doped samples, decreases from 310 K ($x = 0.05$) to 100 K ($x = 0.25$) with increasing $x$. This is much different from that in the single doped samples. The $T_{\mathrm{cs}}^{\mathrm{onset}}$, which is the $T_{\mathrm{c}}^{\mathrm{onset}}$ of the single doped samples and also summarized in Table 1, only slightly changes with increasing doping level.[22] It is also noticed that the transition width $\Delta T$, which is defined as $T_{\mathrm{p}}$–$T_{\mathrm{c}}^{\mathrm{onset}}$($T_{\mathrm{p}}$ is the temperature corresponding to the maximum $M$), also shows different doping dependent behaviour between the single doping and double doping series. With increasing $x$, the $\Delta T$ of the single doped samples is broadened rapidly.[22] But the $\Delta T$ of the double doped samples with $x = 0.20$ and 0.25 is much smaller than that of single doped sample with $x = 0.20$. For $x \leq 0.15$ shown in Fig.3(a), the standard $\lambda$ transition is observed, indicating the cluster-spin glass behaviour. This is similar to that

in the single doped samples.[22] However, for $x = 0.20$ and 0.25 in Fig.3(b), the magnetization is found to decrease at low temperature both in ZFC and FC $M$–$T$ curves, implying a transition to AFM state. The Neél temperature $T_N$ are 45.6 K for $x = 0.20$ and 34.4 K for $x = 0.25$, respectively. These results of the double doped samples seem strange comparing to that for the single doped cases.

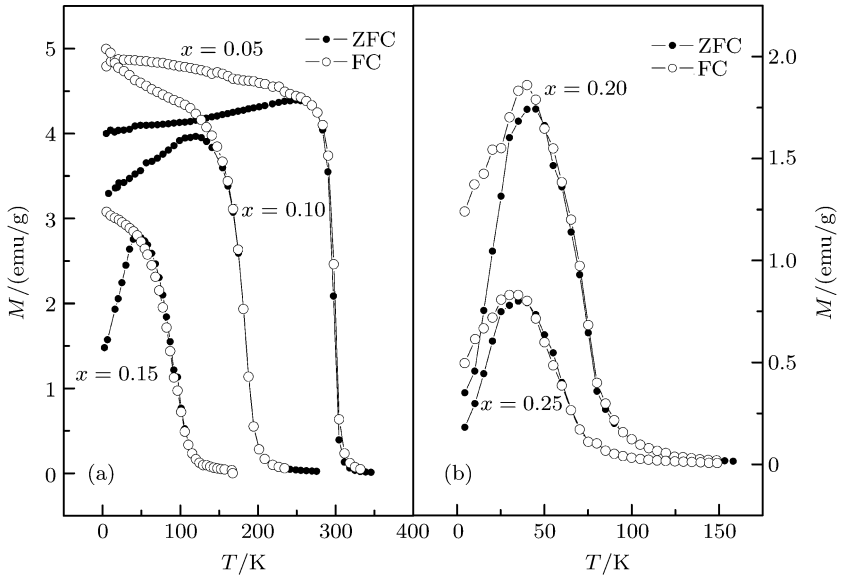



**Fig.3.** Temperature ($T$) dependence of magnetization ($M$) under zero field cooling (ZFC) and field cooling (FC) of $La_{2/3+4x/3}Sr_{1/3-4x/3}Mn_{1-x}Mg_xO_3$ ($0.05 \leq x \leq 0.25$).

In order to get more information, the $M$–$H$ measurements are performed. For single doped samples, typical ferromagnetic behaviour is observed in $M$–$H$ curves for $x = 0.10$ and 0.15.[22] Figure 4 displays the $M$–$H$ relations measured at the typical temperatures for double doped samples. For $x \leq 0.15$, the $M$–$H$ curves show typical FM behaviour, which is similar to the single doped cases.[22] But, for $x = 0.20$ and 0.25, Figs.4(d) and 4(e) show very different results. For $x = 0.20$ in Fig.4(d), the saturated magnetization at 5 K is smaller than that at 60 K. Furthermore, a high-field hysteresis loop is observed in the $M$–$H$ curve at 5 K. The enlargement of the high-field hysteresis loop in the $M$–$H$ curve are shown in Fig.4(f). These facts prove that the samples are in AFM state at low temperature. For $x = 0.25$ in Fig.4(e), the saturated magnetization at 5 K is much smaller than that at 37 K. In addition, the $M$–$H$ curve at 5 K gives the coercive field $H_s$=0.05 T. With temperature increasing, all samples transform into PM phase.

Why there is such large discrepancy between the doping dependent behaviour of $T_c^{onset}$ and $\Delta T$ for the two types of doping? Obviously, the single-doping will not change the average ion radius of A-site. At the same time, the radius of $Mg^{2+}$ is close to that of $Mn^{3+}$. Therefore the tolerance factor $t$ only slightly changes from 0.974 to 0.977 for $x = 0.05$ to 0.20. Thus, the $T_c^{onset}$ is slightly changed. The random distribution $Mg^{2+}$ will transform adjacent $Mn^{3+}$ into $Mn^{4+}$, therefore the sizes of clusters are very different from each other. Therefore, $\Delta T$ is broadened with increasing $Mg^{2+}$ content. In double doped cases, because the average ion radius of A-site changes greatly with the variety of Sr and La content, the $t$ factor is changed drastically with increasing doping level. From Table 1 one can find that the $t$ factor changes from 0.934 to 0.919 for $x = 0.05$ to $x = 0.20$. Thus the $T_c^{onset}$ is greatly suppressed. The double-doping does not create the redundant $Mn^{4+}$ and only $Mg^{2+}$ divides the $Mn^{3+}$–O–$Mn^{4+}$ into clusters. Thus, the difference between each cluster in double doped cases is more slight than that in single doped cases. In addition, the magnetic interaction between the clusters in double doped samples leads to the trend that the PM–FM phase transition occurs consistently. Thus the $\Delta T$ of double doping is smaller than that of single doping.

The different magnetic behaviour between single doping and double doping can be attributed to the different evolution processes of the $Mn^{3+}/Mn^{4+}$ ratio. The single-doping will induce the redundant $Mn^{4+}$.

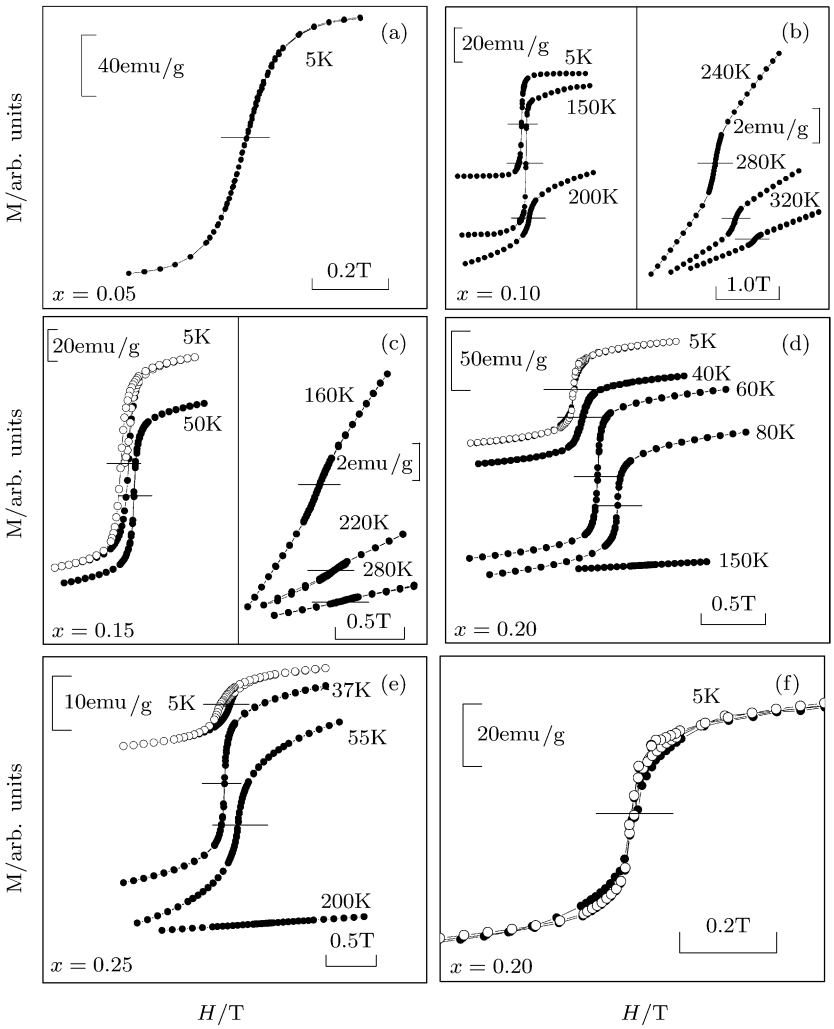



**Fig.4.** Magnetic field ($H$) dependence of magnetization ($M$) of $La_{2/3+4x/3}Sr_{1/3-4x/3}Mn_{1-x}Mg_xO_3$ ($0.05 \leq x \leq 0.25$). The curves are shifted for clarity. The short lines indicate the initial points of each curve.

The non-magnetic $Mg^{2+}$ and the redundant $Mn^{4+}$ around $Mg^{2+}$ will act together to divide $Mn^{3+}$–O–$Mn^{4+}$ into the isolated cluster-spin glass. Thus the standard cluster-spin glass state is observed. Even at $T = 5\,\mathrm{K}$, $H_s$ is very small. However, for double doped samples, the doping will not result in redundant $Mn^{4+}$, thus only $Mg^{2+}$ ions divide the $Mn^{3+}$–O–$Mn^{4+}$ into the FM clusters. The clusters are so close to each other that magnetic interaction may exist between them. The astonishing AFM behaviour observed in Figs.4(d) and 4(e) should be related to this issue. On the one hand, with temperature decreasing, the FM magnetization of the domain in the cluster is strengthened. On the other hand, in order to reach the minimal energy of the system, the interaction between these magnetic domains will compel the domains to rotate to a random arrangement, which results in the decrease of the magnetization. When the temperature is lower than $T_N$=45.6 K for $x = 0.20$ and 34.4 K for $x = 0.25$ respectively, the competition between these two factors results in the decrease of the magnetization. With the temperature decreasing further, the coupling between the domains increases because the FM in the domains is enhanced, therefore the interaction between the domains will be strengthened and thus favours the AFM.

## 3.3. Micromagnetism

As shown in Figs.4(b) and 4(c), an obvious FM component appears at $T = 320\,\mathrm{K}$ and 220 K, far higher than $T_c^{\mathrm{onset}} = 200\,\mathrm{K}$ and 130 K for double doped samples with $x = 0.10$ and 0.15, respectively. Obviously, the magnetism should also be reflected in micromagnetism of the system. Therefore, we measured ESR spectra for double doped samples, as shown in Fig.5.

For double doped samples with $x = 0.05$, as shown in Fig.5(a), there is only the PM lines above $T_c^{onset}$. In Fig.5(d) for $x = 0.20$, all ESR lines can be attributed to PM signals at $T > 110$ K. The ESR lines for $x = 0.25$ are similar to that for $x = 0.20$ and are not shown. All the above phenomena are consistent with the $M$–$T$ relations in Figs.3(a) and 3(d). It must be noticed that in Fig.5(b) for $x = 0.10$ and Fig.5(c) for $x = 0.15$, the PM lines with $g \approx 2$ are always accompanied by a weak FM line with $g > 2$ marked by ▲ at $T > T_c^{onset}$. For $x = 0.10$, the FM signal appears between 200 K and 340 K, which is much higher than $T_c^{onset}$=200 K. For $x = 0.15$, the FM peaks are observed between 140K and 260K ($T_c^{onset} = 130$ K). These results indicate that a weak FM phase is embedded in the PM matrix above $T_c^{onset}$.[25–29] It is also noticed that the FM signal in $x = 0.10$ is more evident than that in $x = 0.15$. In contrast, in single doped samples one can find that there is only PM lines above $T_c^{onset}$ and the FM lines appear instantaneous below $T_c^{onset}$.[22]

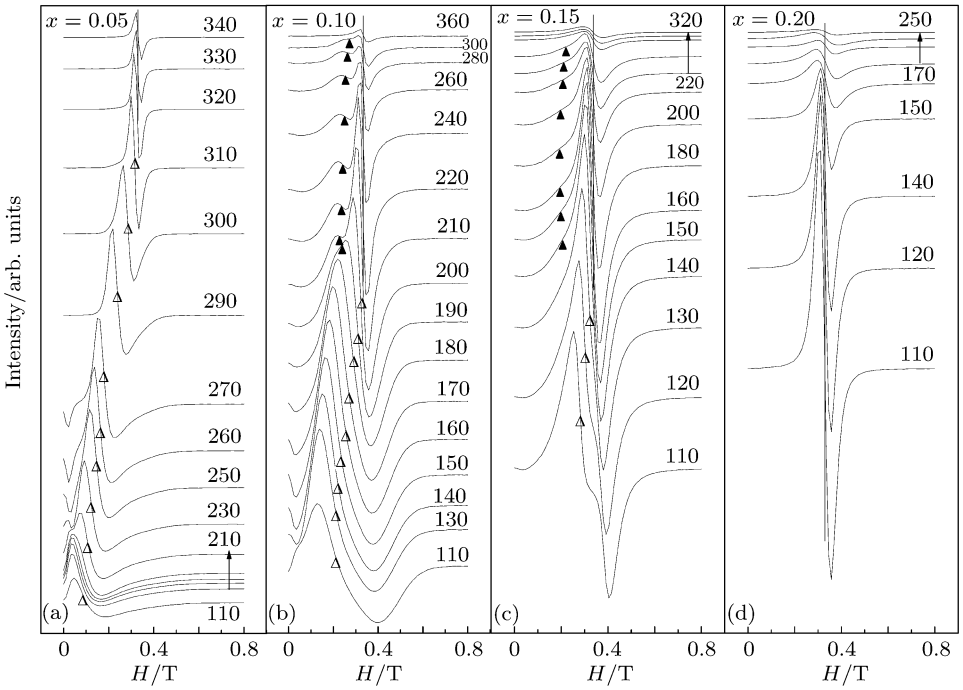



**Fig.5.** ESR spectra of $La_{2/3+4x/3}Sr_{1/3-4x/3}Mn_{1-x}Mg_xO_3$ ($0.05 \leq x \leq 0.20$).

It is very strange that the phase separation is observed only in double doped cases. As we know, for single doped series, the $Mn^{3+}/Mn^{4+}$ ratio changes from 2 : 1 ($x = 0.00$) to 1 : 2 ($x = 0.20$). $T_c^{onset}$ is 360 K for $La_{2/3}Sr_{1/3}MnO_3$ and is still about 320K even at $x = 0.20$. This can be attributed to the fact that the tolerance factor $t$, Mn–O bond length $L_{Mn-O}$ and Mn–O–Mn bond angle $\theta_{Mn-O-Mn}$ are not changed greatly with Mg doping (see Table 1). However, in double doped cases, although the ratio of $Mn^{3+}/Mn^{4+}$ is always equal to 2 : 1, the $t$ factor, $L_{Mn-O}$ and $\theta_{Mn-O-Mn}$ are changed greatly with decreasing Sr content (see Table 1). Thus $T_c$ and $T_c^{onset}$ are suppressed drastically. It must be emphasized that the $t$ factor, $L_{Mn-O}$ and $\theta_{Mn-O-Mn}$ in Table 1 are all average values. For $x = 0.05$, although Sr content decreases a little and the microstructure is slightly distorted, $La_{2/3}Sr_{1/3}Mn_{1-x}Mg_xO_3$ with $Mn^{3+}/Mn^{4+}$=2 : 1 still dominates the whole system, thus the $M$–$T$ behaviour of Fig.3(a) is very similar to that for $x = 0.0$[22] except for $T_c$ and $T_c^{onset}$ which are dominated by average effect of $t$, $L_{Mn-O}$ and $\theta_{Mn-O-Mn}$. For $x = 0.10$ and 0.15, although the $t$ factor, $L_{Mn-O}$ and $\theta_{Mn-O-Mn}$ are changed in some degree, there still exist $La_{2/3}Sr_{1/3}Mn_{1-x}Mg_xO_3$ with $Mn^{3+}/Mn^{4+}$=2 : 1 in some small regions. In these small regions, $T_c$ is maintained at high temperature which is little lower than 360 K. Therefore, in ESR spectra these small FM zone with high $T_c$ are detected in PM background at $T > T_c^{onset}$. For $x \geq 0.20$, these small $La_{2/3}Sr_{1/3}Mn_{1-x}Mg_xO_3$ regions are greatly reduced and almost disappear. Thus, there exists no FM phase at $T > T_c^{onset}$ and only PM line is observed for $x \leq 0.20$.

### 3.4. Thermal activation and VRH mechanism

Figure 6 shows the resistivity as a function of temperature ($\rho$–$T$) for all the double doped samples. For $x = 0.05$, $\rho$–$T$ curve exhibits metallic behaviour at $T < 310\,\mathrm{K}$ because it is in FM state. For $x = 0.10$, an inflection is observed in $\rho$–$T$ curve. When $x \geq 0.15$, the samples display semiconductor-like transport behaviour in the whole temperature range. The resistivity increases quickly with doping level.

In order to understand the mechanism lying behind the transport behaviours, we use the thermal activation model[30] and variable-range hopping (VRH) model[31] to fit the $\rho$–$T$ curves. In Fig.7, the zero-field $\rho(T)$ curves are replotted as $\rho$–$T^{-1}$ and $\rho$–$T^{-1/4}$, respectively.

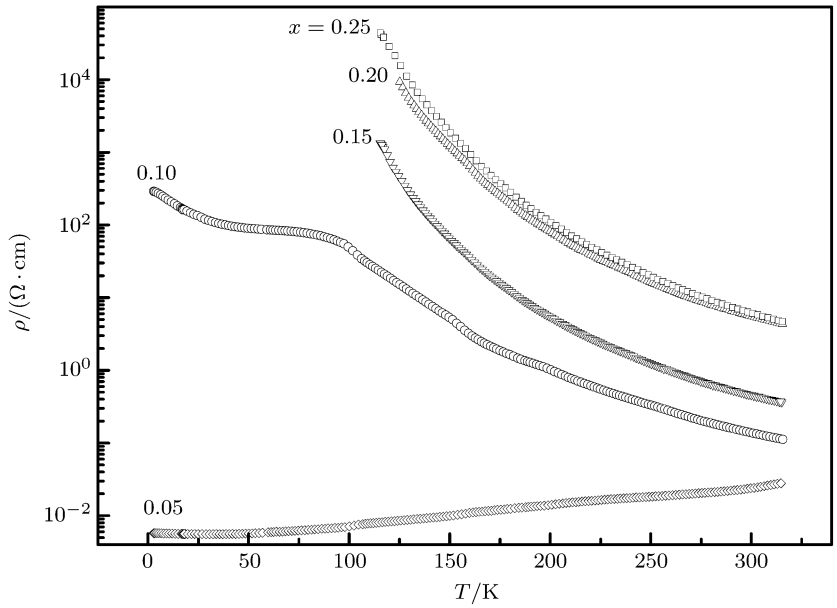



**Fig.6.** Temperature ($T$) dependence of resistivity $\rho$ in zero magnetic field of $La_{2/3+4x/3}Sr_{1/3-4x/3}Mn_{1-x}Mg_xO_3$ ($0.05 \leq x \leq 0.25$).

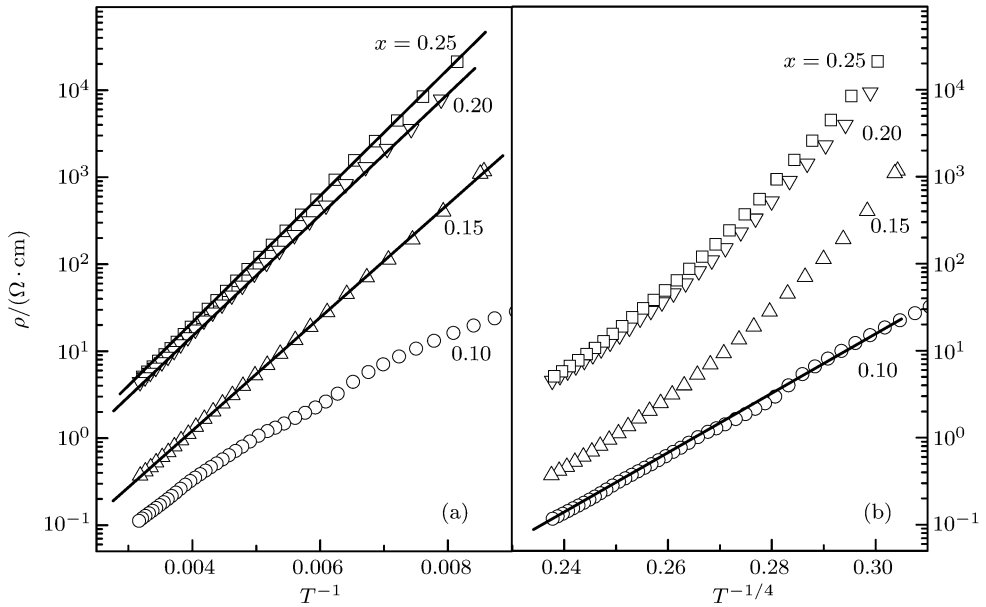



**Fig.7.** Zero-field resistivity curves of $La_{2/3+4x/3}Sr_{1/3-4x/3}Mn_{1-x}Mg_xO_3$ ($0.05 \leq x \leq 0.25$) replotted as $\rho \sim T^{-1}$ (a) and $\rho \sim T^{-1/4}$ (b), respectively.

The $\rho$–$T$ curves for $x \geq 0.15$ are well fitted by thermal activation model in the high temperature region, as shown in Fig.7(a). But for $x = 0.10$, the high temperature $\rho$–$T$ behaviour can only be fitted by VRH model, as shown in Fig.7(b). As is known, for $x = 0.10$, the FM phase are embedded in the PM background at

$T > T_c^{onset}$. This will induce random magnetic potential. Therefore, the VRH mechanism dominates in high temperature region for $x = 0.10$. For $x = 0.15$, although there is also the phase separation, but as evidenced in ESR results, the FM is very weak. It is too weak to form sufficient random magnetic potential. One can find from the ESR results in Fig.5(c) that the system is mainly the PM phase at $T > T_c^{onset} = 130$K. So the transport behaviour for $x = 0.15$ is dominated by thermal activation process at $T > 130$ K. The same argument applies for the $x = 0.15$, 0.20 and 0.25 cases, where only PM lines are observed in ESR. Therefore, the thermal activation model is more suitable for them.

## 4. Conclusion

In summary, the double doped $La_{2/3+4x/3}Sr_{1/3-4x/3}Mn_{1-x}Mg_xO_3$ samples with fixed $Mn^{3+}/Mn^{4+} = 2/1$ is studied by means of magnetism and transport measurements. $T_c^{onset}$ is found to be suppressed drastically in double doped samples, which is attributed to the variation of $t$ factor. For $x = 0.10$ and 0.15, phase separation is observed at temperatures higher than $T_c^{onset}$. Phase separation is rather strong for $x = 0.10$ and results in drastic random magnetic potential. Thus, carriers are localized and VRH process dominates in the high temperature region. For other samples, sufficient random potential is not induced because there is no or only weak phase separation. Therefore, thermal activation mechanism is responsible for the transport behaviour in high temperature region. For $x = 0.20$ and 0.25, unexpected AFM behaviours are observed at low temperature. The results reported here are found to be much different from that of the single doped cases[22] and can only be understood by considering the special role of double doping. The results obtained have deepened our knowledge of the role of the double doping and the differences between single doping and double doping.

## References


[1] von Helmolt R, Wecker J, Holzapfel B, Schultz L and Samwer K 1993 *Phys. Rev. Lett.* **71** 2331

[2] Jin S, Teifel T H, McCormack M, Fastnacht R A, Ramesh R and Chen L H 1996 *Science* **273** 880

[3] Singh D J and Pickett W E 1998 *Phys. Rev.* B **57** 88

[4] Hemberger J, Krimmel A, Kurz T, Krug von Nidda H A, Ivanov V Yu, Mukhin A A, Balbashov A M and Loidl A 2002 *Phys. Rev.* B **66** 094410

[5] Maezono R, Ishihara S and Nagaosa N 1998 *Phys. Rev.* B **58** 11583

[6] Chen X, Wang Z H, Li R W, Shen B G, Zhao H W and Zhan W S 2001 *Chin. Phys.* **10** 751

[7] Lu Y, Li Q A, Di N L, Ma X and Cheng Z H 2003 *Chin. Phys.* **12** 789

[8] Zhao K, Feng J F, Huang Y H and Huang K Q 2005 *Chin. Phys.* **14** 398

[9] Liu X B, Zhang S Y, Shen B G, Yao J L and Wang F 2004 *Chin. Phys.* **13** 1139

[10] Xiao C T, Han L A, Xue D S and Zhao J H 2003 *Acta Phys. Sin.* **52** 1245 (in Chinese)

[11] Duan P, Chen Z H, Dai S Y, Zhou Y L and Lv H B 2006 *Acta Phys. Sin.* **55** 1441 (in Chinese)

[12] Tan G T, Chen Z H and Zhang X Z 2005 *Acta Phys. Sin.* **54** 379 (in Chinese)

[13] Ahn K H, Wu X W, Liu K and Chien C L 1996 *Phys. Rev.* B **54** 15299

[14] Sun Y, Xu X J and Zhang Y H 2000 *Phys. Rev.* B **63** 54404

[15] Gayathri N, Raychaudhuri A K and Tiwary A K 1997 *Phys. Rev.* B **56** 1345

[16] Zener C 1951 *Phys. Rev.* **82** 403

[17] Millis A J, Littlewood P B and Shraiman B J 1995 *Phys. Rev. Lett.* **74** 5144

[18] Millis A J 1996 *Phys. Rev.* B **53** 8434

[19] Zhou J S and Goodenough J B 1998 *Phys. Rev. Lett.* **80** 2665

[20] Kou Z Q, Di N L, Ma X, Li Q A and Cheng Z H 2005 *Chin. Phys.* **14** 1653

[21] Kou Z Q, Di N L, Lu Y, Ma X, Li Q A and Cheng Z H 2005 *Chin. Phys.* **14** 311

[22] Fan J Y, Pi L, Tong W, Xu S J, Gao J, Zha C Z and Zhang Y H 2003 *Phys. Rev.* B **68** 092407

[23] Rao G H, Sun J R and Liang J K 1997 *J. Appl. Phys.* **82** 4687

[24] Zhou J P, McDevitt J T, Zhou J S, Yin H Q, Goodenough J B, Gim Y and Jia Q X 1999 *Appl. Phys. Lett.* **75** 1147

[25] Allodi G, De Renzi R, Guidi G, Licci F and Pieper M W 1997 *Phys. Rev.* B **56** 6036

[26] Ibarra M R, Zhao G, De Teresa J M, Garcia-Landa B, Arnold Z, Marquina C, Algarabel P A, Keller H and Ritter C 1998 *Phys. Rev.* B **57** 7446

[27] Mori S, Chen C H and Cheong S W 1998 *Phys. Rev. Lett.* **81** 3972

[28] Uehara M, Mori S, Chen C H and Cheong S W 1999 *Nature* **399** 560

[29] Moreo A, Yunoki S and Dagotto E 1999 *Science* **283** 2034

[30] Kusters R M, Singleton J and Keen D A 1989 *Physica* B **155** 362

[31] Viret M, Ranno L and Coey J M D 1997 *Phys. Rev.* B **55** 8067